Journal of Power Sources 264 (2014) 76–82

Contents lists available at ScienceDirect

Journal of Power Sources

journal homepage: www.elsevier.com/locate/jpowsour

Pt–Co nanostructures electrodeposited on graphene nanosheets for methanol electrooxidation

Reza Ojani*, Jahan-Bakhsh Raoof, Mona Goli, Roudabeh Valiollahi

Electroanalytical Chemistry Research Laboratory, Department of Analytical Chemistry, Faculty of Chemistry, University of Mazandaran, 47416-95447 Babolsar, Iran

HIGHLIGHTS

- Co nanoparticles were electrodeposited on graphene modified GC electrode (Co/G/GC).
- Pt–Co nanostructures were loaded on Co/G/GC by galvanic replacement reaction.
- The physical and electrochemical properties of Pt–Co/G/GC were investigated.
- The Pt–Co/G was used as the anode electrocatalyst for methanol electrooxidation.
- The onset potential of methanol oxidation at Pt–Co/G/GC occurred at low potential.

ARTICLE INFO

Article history:
Received 12 October 2013
Received in revised form
18 March 2014
Accepted 29 March 2014
Available online 18 April 2014

Keywords:
Pt–Co nanostructures
Graphene nanosheets
Electro-deposition
Galvanic replacement
Methanol electrooxidation

ABSTRACT

Glassy carbon electrode modified by Pt–Co nanostructures decorated on graphene nanosheets (Pt–Co/G/GCE), is fabricated. Co nanostructures are electro-deposited on graphene modified GC electrode and then Pt nanostructures are loaded on the surface of modified electrode by galvanic replacement reaction between Co nanostructures and H_2PtCl_6. The physical and electrochemical properties of Pt–Co/G/GCE are investigated by scanning electron microscopy, energy dispersive X-ray, cyclic voltammetry and chronoamperometry. The morphology of as-prepared graphene nanosheets is investigated by transmission electron microscopy. The prepared Pt–Co/G is used as the anode electrocatalyst for methanol electrooxidation. The fabricated electrocatalyst exhibits an enhanced electrocatlytic performance for methanol electrooxidation.

1. Introduction

Fuel cells are promising efficient alternative energy sources for portable and vehicular applications. Among various types of fuel cells, direct methanol fuel cells (DMFCs) have attracted much more attentions due to their interesting properties such as low operating temperature, high power density and relatively quick start-up [1–4]. However, the practical development of DMFCs is limited by poor activity of methanol electrooxidation activity and high cost of noble metal catalysts [1]. Metal and semiconductor nanoparticles have attracted tremendous attention in various fields such as catalysis, photography, optics, biological and chemical sensor [5–8]. Pt and its alloy nanoparticles are among the best electrocatalysts for methanol electrooxidation [9]. There are different approaches to improve the electrocatalytic activity of a catalyst toward methanol electrooxidation such as incorporation of a second element to Pt or controlling the morphology (size and shape) [10–14]. Recently, many researchers have developed Pt-based alloy catalysts with high activity for the oxygen reduction reaction (ORR) such as Pt–Ru, Pt–Pd, Pt–Co and Pt–Sn [15–17]. Besides, these Pt-based alloy catalysts have good tolerance to CO poisoning as compared with pure Pt [18,19]. It has been found that Pt–Co alloys have high activity and excellent tolerance to CO poisoning in comparison with pure Pt catalysts [20–22], and Co is much cheaper than precious metal Ru.

Support effects are well known to affect catalyst activity. So, the support materials have an important role in catalytic behavior of catalyst. The supporting materials and their surface conditions highly affect catalytic activity of the Pt catalyst [23]. The supporting materials with high surface area reduce the metal loading while

* Corresponding author. Tel.: +98 112 5342301; fax: +98 112 5342302.
E-mail address: Fer-o@umz.ac.ir (R. Ojani).

http://dx.doi.org/10.1016/j.jpowsour.2014.03.147
0378-7753/

keeping the high catalytic activity. Recently, graphene, one of the carbon materials, has been a good candidate as support materials [24–26]. Graphene has gained interests in many fields of application, because of its unique electronic, optical and chemical properties and its potential applications in nanomaterials and nanotechnology [27]. The-two dimensional layered structure of graphene, provides large specific surface area, which makes it suitable for immobilizing various substances such as metal, nanoparticles, biomolecules and etc. Electron transfer through graphene is sensitive to adsorbed molecules, because every atom in a graphene is a surface atom [28]. When graphene is used as an electrode, the electron transfer is promoted which makes graphene an inexpensive alternative to carbon nanotubes [29]. Also, the layered structure of graphene makes it possible to use both sides of it as support for catalysts; this makes graphene a promising catalyst carrier [30].

Galvanic replacement reaction (GRR) is a type of electroless deposition. In a chemical oxidation–reduction reaction, metal ions with higher standard potential are reduced and templates with lower standard potentials are oxidized [31]. Recently, it has been proved that this simple and spontaneous process is an attractive approach for the growth of structures directly on metal or semiconductor substrates such as deposition of Au on Si [32], Ag/Pd on Si [33], Cu on Si [34], Pt on Ti [35], Au on Ge [36], Pt on Ge [37], Cu on TaN [38], Cu on Al [39], Zn on Al [40], Ni on Al [41], Pd on Ag [42], Pt/Au on Cu [43], Au on Cu [44], Ag on Cu [45], and Au on Ag [46], and other combinations.

Therefore, in the present work, with respect to advantages of graphene nanosheets and galvanic replacement reaction, the modified electrode was prepared by galvanic replacement. In this way, we report a simple and rapid route for preparation of the bimetallic Pt–Co catalyst through a method based on partially replacement of metallic Co by Pt using immersion of the Co/G/GCE in H_2PtCl_6 solution. The general objective of the present work is to obtain the Pt–Co/G/GCE for electrocatalytic oxidation of methanol which has significant attraction in DMFCs.

2. Experimental

2.1. Chemical and reagents

The solvent used for the electrochemical studies was twice distilled water. Graphite powder (particle diameter = 0.1 mm), sulfuric acid, hexachloroplatinic (IV) acid hexahydrate, cobalt (II) sulfate heptahydrate and methanol were purchased from Merck. Sodium hydroxide was purchased from Fluka.

2.2. Instrumentation

Scanning electron microscopy and energy-dispersive X-ray analysis (EDX) were done using KYKY-EM3200 and VEGA – TESCAN – XMU electron microscope. The morphology of graphene was determined by a PHILIPS CM30 transmission electron microscopy (TEM). Electrochemical studies were performed in a three-electrode cell with Pt–Co/G/GC as working electrode, a Pt wire as counter electrode and Ag|AgCl as reference electrode using a computer-controlled potentiostat/galvanostat (μ-Autolab TYPE III, Eco Chemie BV, Netherlands).

2.3. Preparation of graphene nanosheets

Graphene oxide (GO) was prepared with the Hummers method and purified [47], then chemical reduction of GO to graphene was carried out [48]. Fig. 1 shows TEM image of graphene nanosheets. As can be seen, they are rippled like a silk weave due to extremely small thickness of graphene, suggesting a flexible structure of graphene sheets.

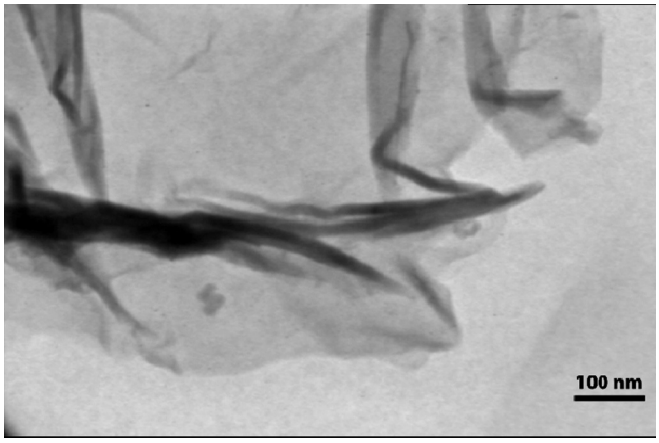

Fig. 1. TEM image of graphene nanosheets.

2.4. Preparation of Pt–Co/G/GCE

GC electrode was polished with alumina slurry down to 0.05 μm on a polishing cloth followed by sonicating in distilled water and absolute ethanol. 1.0 mg graphene was dispersed in 1.0 mL water using high power ultrasound. A 5.0 μL portion of the resulting graphene nanosheets dispersion was measured and the syringe was put over the GC electrode. The graphene sheet suspension was then dropped on the electrode, which was dried in an oven (70 °C) to evaporate the solvent. The resultant was graphene nanosheets modified GC electrode (G/GCE). For electro-deposition of Co nanostructures on G/GCE, the fabricated G/GC electrode was immersed in 0.02 M $CoSO_4$ + 0.1 M Na_2SO_4 solution. A cyclic scan in the potential range from 0.6 V to −1.0 V was performed (Fig. 2) as mentioned elsewhere [49] and the Co nanostructures modified G/GC electrode (Co/G/GCE) was obtained. The oxidation peak at −0.33 V is attributed to oxidation of electrodeposited Co nanostructures on Co/G/GCE and the reduction peak at −0.86 V is due to reduction of Co^{2+} on the Co/G/GCE. Owing to increase in amount of the electrodeposited Co nanostructures caused by increasing the

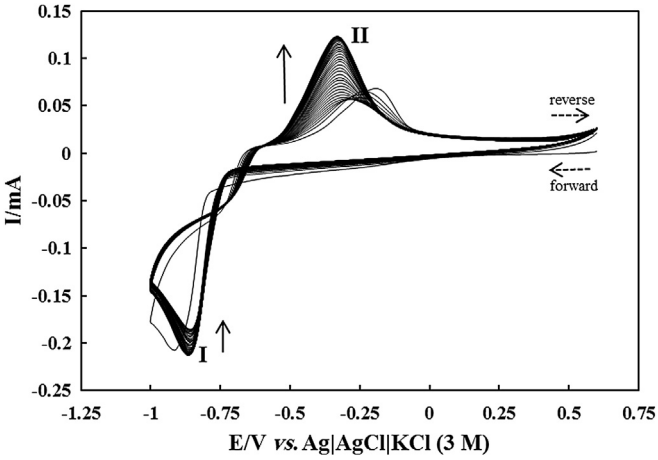

Fig. 2. CVs of graphene/GCE in 0.02 M $CoSO_4$ + 0.1 M Na_2SO_4 at $\nu = 50$ mV s^{-1}, number of potential cycles: 45.

cycle number, the oxidation peak current is increased and the reduction peak current is decreased [49].

Pt nanostructures were decorated on Co/G/GCE by immersing the modified electrode in 1.0 mM H_2PtCl_6 solution. By the galvanic replacement according to Eq. (1), Co nanostructures are oxidized to Co^{2+} and Pt (IV) is reduced to metallic Pt.

$$2Co + PtCl_6^{2-} \rightarrow Pt + 2Co^{2+} + 6Cl^- \quad (1)$$

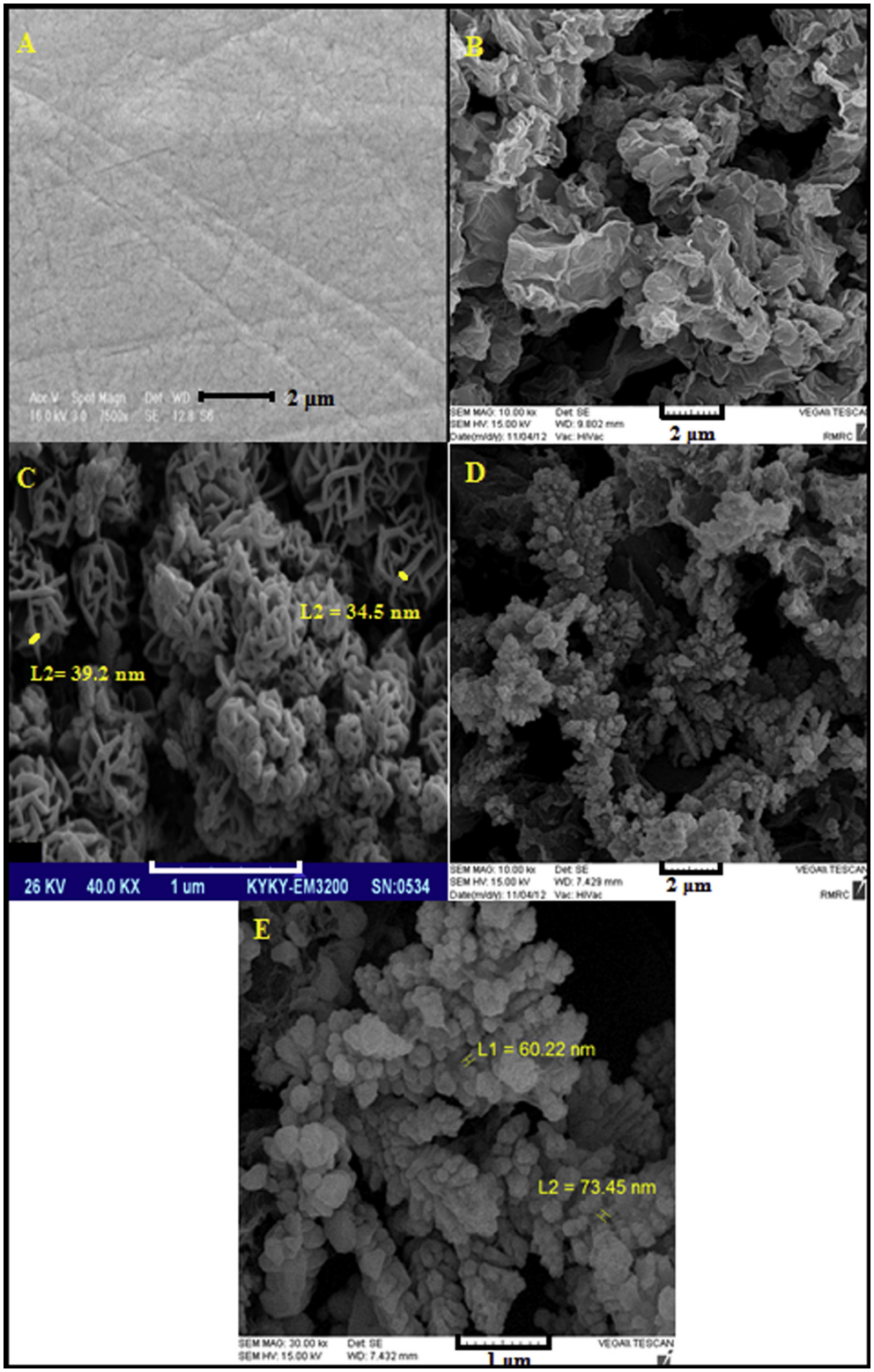

Fig. 3. The SEM images of: (A) bare GCE, (B) G/GCE, (C) Co/G/GCE, (D) Pt–Co/G/GCE and (E) the high magnification SEM image of Pt–Co/G/GC.

After partial replacement, the modified electrode was rinsed with doubly distilled water. At beginning of experiments, the modified electrodes were immersed in 0.5 M H_2SO_4 solution and the potentials was cycled between −0.3 and 1.2 V until reproducible cyclic voltammograms were attained.

3. Results and discussion

3.1. Morphology and characterization

Fig. 3 depicts the SEM image of electrode surface at each step of modification. Fig. 3A shows SEM image of bare GC electrode surface, which demonstrates that the surface is smooth and homogeneous. Fig. 3B shows the SEM image of electrode surface after coating the GC electrode by graphene nanosheets. Graphene layers at the surface of GC can be seen obviously. The SEM image after electro-deposition of Co nanostructures at the G/GCE is shown in Fig. 3C. As can be observed, Co nanostructures with average size of 37 nm are deposited at the edge of graphene. So, after replacement of Co with the Pt, SEM image shows that (Fig. 3D), Pt–Co nanostructures were placed at the edge of graphene. Fig. 3E shows high magnification SEM image of Pt–Co/G/GC with average nanostructures size of 67 nm. The decorated Pt–Co exists as cluster and cauliflower like nanostructures.

In order to determine chemical compositions of as-prepared Pt–Co/G, EDX analysis was performed. Fig. 4 shows EDX spectra and elemental percentages for Pt–Co/G. Results reveal that the Pt and Co mass percentage is 33.57% and 1.28%, respectively. From the EDX results, Pt is the major element. Carbon is derived from the graphene nanosheets. Oxygen may come from the working electrode substrate or electrolyte solution.

3.2. Optimization of galvanic replacement reaction time

Electrode response toward methanol electrooxidation depends on the amount of loaded Pt on the modified electrode. On the other hand, the amount of loaded Pt is directly proportional to replacement reaction time. Hence, the replacement reaction was performed at different times and then electrooxidation of methanol was investigated at the prepared modified electrode. As can be observed in Fig. 5, current density of methanol oxidation increases with increasing galvanic replacement reaction time up to 120 s due to increment in amount of loaded Pt. With further increase in galvanic replacement reaction time, the methanol oxidation peak current drops. One possible explanation could be significant decrease in Pt real surface area at higher times. On the other hand, as the galvanic replacement is surface limited, the amount of loaded Pt and consequently active surface area do not show significant changes. On the basis of the result, 120 s is enough to saturate the electrode surface by incorporated Pt particles that enhance the methanol oxidation process. So, 120 s was selected as the replacement reaction time for further studies.

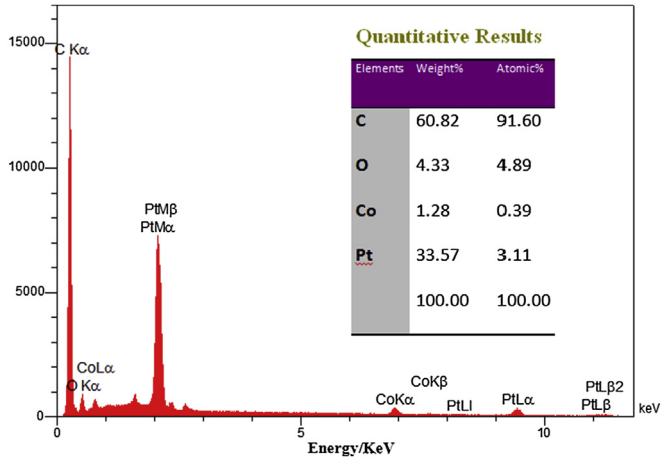

Fig. 4. Energy dispersive X-ray (EDX) of the Pt–Co/G/GCE.

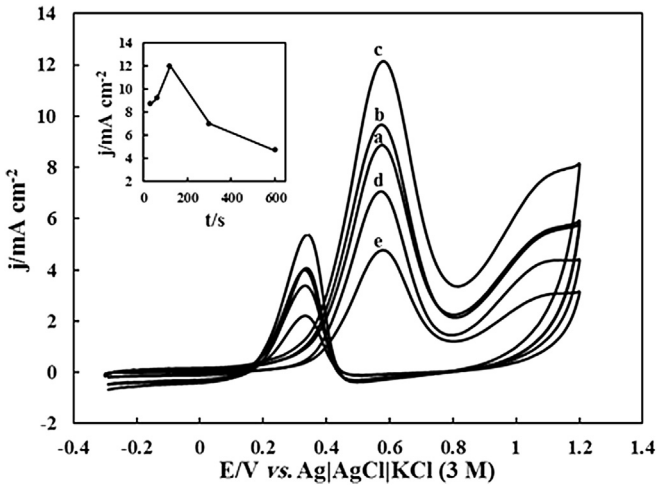

Fig. 5. Cyclic voltammograms of Pt–Co/G/GC electrodes prepared at various galvanic replacement time [(a) 30 s, (b) 60 s, (c) 120 s, (d) 300 s and (e) 600 s] in 0.5 M H_2SO_4 solution in the presence of 1.0 M methanol, in the potential range from −0.3 V to 1.2 V at $\nu = 50$ mV s^{-1}. Inset: variation of the electrocatalytic current density of methanol *vs.* time of galvanic exchange reactions.

3.3. Active surface area estimation

Active surface area of Pt–Co/G/GCE could be estimated from coulombic charge for hydrogen adsorption and desorption, as obtained from cyclic voltammetry in H_2SO_4 0.5 M (dashed line in Fig. 6) according to Eq. (2), where Q_H is average charge of hydrogen adsorption/desorption and 210 μC cm^{-2} is the charge associated with a monolayer of adsorbed hydrogen [50–52].

$$A_r = QH/210\mu C\ cm^{-2} \quad (2)$$

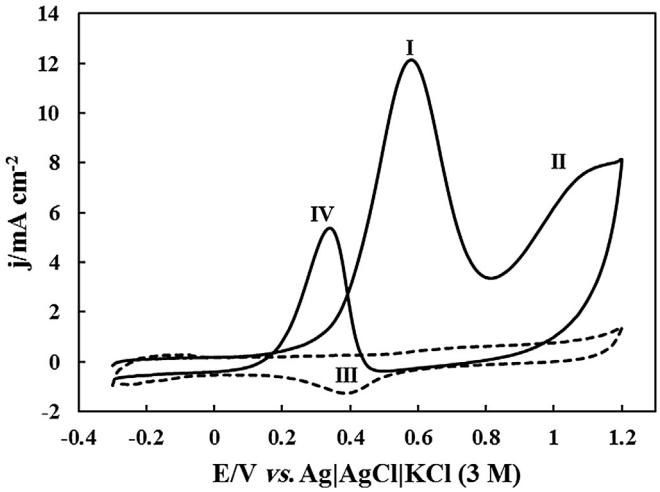

Fig. 6. Electrochemical responses of Pt–Co/G/GCE in 0.5 M H_2SO_4 (dash line) in the absence and (solid line) the presence of 1.0 M methanol, in the potential range from −0.3 V to 1.2 V at $\nu = 50$ mV s^{-1}.

Table 1
Comparison of methanol electrocatalytic oxidation at the surface of some modified electrodes containing Pt nanoparticles.

Electrode	Modifier	Me concentration (M)	Electrolyte concentration (M)	Scan rate (mV s^{-1})	E_{op}[a] (V)	References
GCE	Pt–polyaniline	0.5	0.5	5	0.30	[59]
Au	Pt–polypyrrole	1.0	0.1	50	0.40	[60]
Al	Pt/PoAP[b]	0.10	0.1	20	0.20	[54]
GCE	Pt–silica	0.05	0.1	50	0.24	[61]
Ti	Pt nanorods	2.0	0.5	50	0.30	[62]
GCE	nc-Pt/nr-PAANI[c]	0.5	0.5	50	0.30	[63]
SWCNT	Pt nanoparticles	2.0	1.0	50	0.30	[64]
GCE	RGO[d]-Pt–Co	2.0	0.1	25	0.28	[65]
Au	MPPt/Ru[e]	1.0	1.0	20	0.55	[66]
GCE	Pt–Co/G[f]	1.0	0.5	50	0.10	This work

[a] Onset potential.
[b] Poly(*o*-aminophenol).
[c] Poly(*N*-acetylaniline) nanorods/platinum nanoclusters.
[d] Reduced graphene oxide.
[e] Mesoporous Pt (MPPt) modified by adsorbed Ru.
[f] Pt–Co nanostructures decorated on graphene nanosheets.

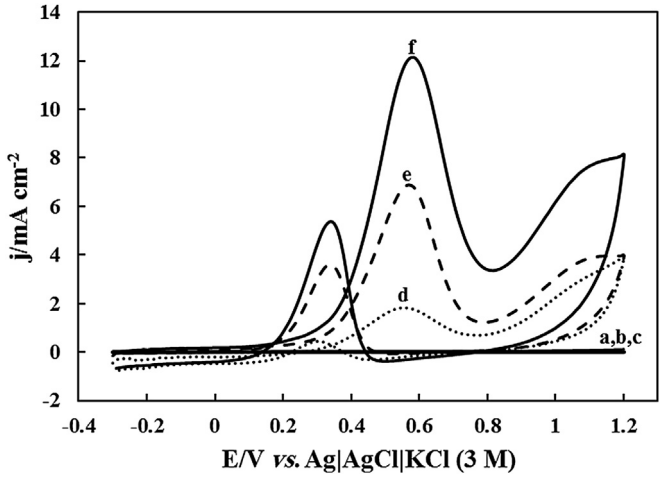

Fig. 7. Cyclic voltammograms of (a) GCE, (b) G/GCE, (c) Co/G/GCE, (d) bulk Pt, (e) Pt–Co/GCE and (f) Pt–Co/G/GCE in 0.5 M H_2SO_4 + 1.0 M methanol, in the potential range from −0.3 V to 1.2 V at $\nu = 50$ mV s^{-1}.

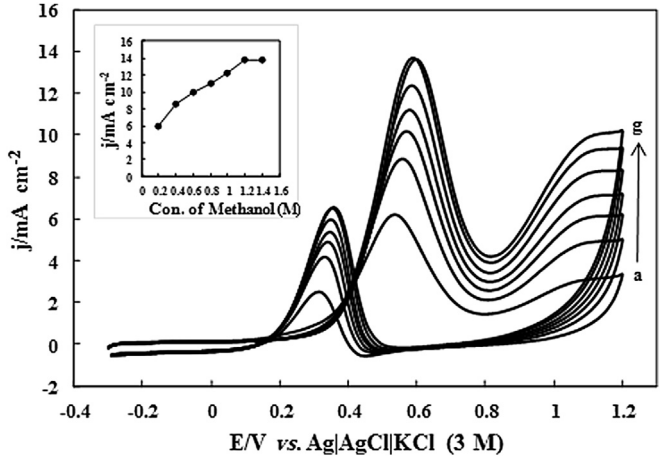

Fig. 8. Current density–potential curves of 0.5 M H_2SO_4 solution with different concentrations of methanol (a) 0.2, (b) 0.4, (c) 0.6, (d) 0.8, (e) 1.0, (f) 1.2 and (g) 1.4 M at the Pt–Co/G/GCE, in the potential range from −0.3 V to 1.2 V at $\nu = 50$ mV s^{-1}. Inset: plot of the dependence of methanol oxidation peak current density on the methanol concentration.

The active surface area is estimated at 0.053 cm^{-2} and the amount of the loaded Pt was calculated as 0.30 mg cm^{-2} from EDX spectra.

3.4. Electrocatalytic behavior of Pt–Co/G/GC

Fig. 6 shows electrochemical behavior of Pt–Co/G/GC electrode in H_2SO_4 0.5 M in absence (dashed line) and presence (solid line) of 1.0 M methanol in the potential range of −0.3 V to 1.2 V at a sweep rate of 50 mV s^{-1}. The anodic current density of methanol oxidation started from 0.10 V with low anodic current and by sweeping to the more positive potentials, the anodic peak current is maximum at about 0.55 V (peak I). The oxidation peak current decreases at more positive potentials than region I due to the formation of platinum oxide and a broad anodic peak (II) appears. When the potential scan is reversed, a reduction peak III appears, which is due to the reduction of platinum oxide to Pt and clean platinum becomes available. The methanol oxidation takes place more easily at the surface of clean platinum and therefore the peak current IV for methanol oxidation appears [53]. The height of this peak depends on the residual poisoning species on platinum surface that can be removed [54]. As mentioned in the literature, Pt–Co alloys have high activity and excellent tolerance to CO poisoning in comparison with pure Pt catalysts [21,22,55,56]. It seems that the good

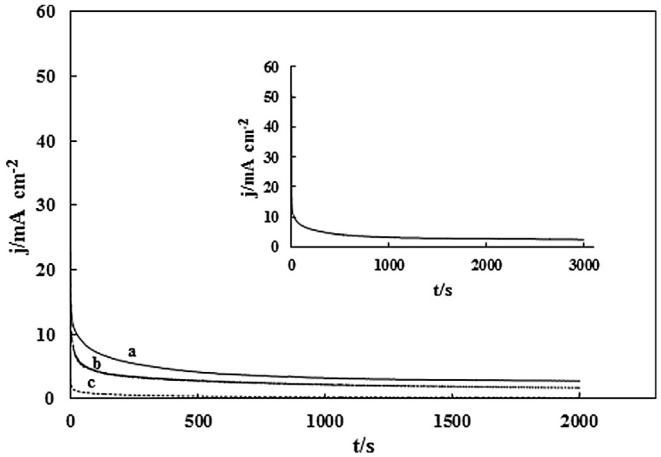

Fig. 9. Chronoamperometry of (a) Pt–Co/G/GCE, (b) Pt–Co/GCE and (c) bulk Pt in a solution of 1.0 M methanol + 0.5 M H_2SO_4, the electrode potential was held at 0.62 V for 2000 s. Inset: chronoamperometry of the Pt–Co/G/GCE in a solution of 1.0 M methanol + 0.5 M H_2SO_4, the electrode potential was held at 0.62 V for 3000 s.

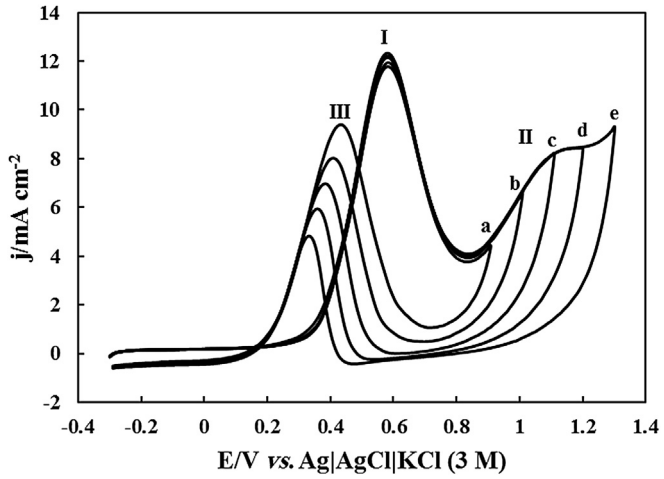

Fig. 10. The effect of upper limit of potential scanning region on the electrooxidation of 1.0 M methanol in 0.5 M H_2SO_4 solution at the Pt–Co/G/GCE at $\nu = 50$ mV s^{-1} (a) 0.9, (b) 1.0, (c) 1.1, (d) 1.2 and (e) 1.3 V.

electrocatalytic behavior of the modified electrode is due to the synergic effect of Pt and Co and its integration with good conductivity of graphene.

In Table 1, the onset potential of methanol electrooxidation in acidic medium at different electrodes containing Pt nanoparticles is shown. As can be seen, the onset potential at the prepared electrode (Pt–Co/G/GCE) is less positive than others.

For comparison, methanol electrooxidation was also studied at bare GCE, G/GCE, Co/G/GCE and bulk Pt electrode. The obtained results are shown in Fig. 7. The methanol electrooxidation is observed only at Pt–Co/G/GC and bulk Pt electrodes, while at Pt–Co/G/GCE the current density is higher than at the bulk Pt electrode. This could be attributed to the nanostructured Pt–Co. For investigation of graphene effect on electrocatalytic behavior of modified electrode, Pt–Co/GCE was prepared. The results show that current density at Pt–Co/G/GCE is higher than at Pt–Co/GCE. This reveals that existence of graphene nanosheets improves the electrocatalytic activity of modified electrode.

3.5. Effect of methanol concentration

Cyclic voltammograms of Pt–Co/G/GCE at various concentrations of methanol were recorded in 0.5 M H_2SO_4 and in the potential range of −0.3 V to 1.2 V at a sweep rate of 50 mV s^{-1} (Fig. 8). In inset of Fig. 8, it is clearly observed that the anodic current increases as methanol concentration increases and levels off at concentrations higher than 1.2 M. This effect is assumed to be caused by the saturation of active sites at the surface of electrode. In accordance with this result, to obtain a higher peak current density, the optimum concentration of methanol is about 1.2 M.

3.6. Long-term stability of the Pt–Co/G/GCE

In the practical view, long-term stability of the electrode is important. For evaluation of the catalytic activity and stability of the electrodes, chronoamperograms were recorded for a period of time (2000 s) for the oxidation of 1.0 M methanol + H_2SO_4 0.5 M at the surfaces of (a) Pt–Co/G/GCE, (b) Pt–Co/GCE and (c) bulk Pt (Fig. 9). From the obtained results, the higher oxidation current density is obtained at the Pt–Co/G/GCE. This could be due to higher surface area and good conductivity of graphene, and electrocatalytic activity of Pt–Co/G/GCE. Also, inset of this figure shows typical chronoamperogram curve for 3000 s for methanol electrooxidation at the surface of Pt–Co/G/GCE. As can be seen, the current density decreased in the first seconds and then reaches steady-

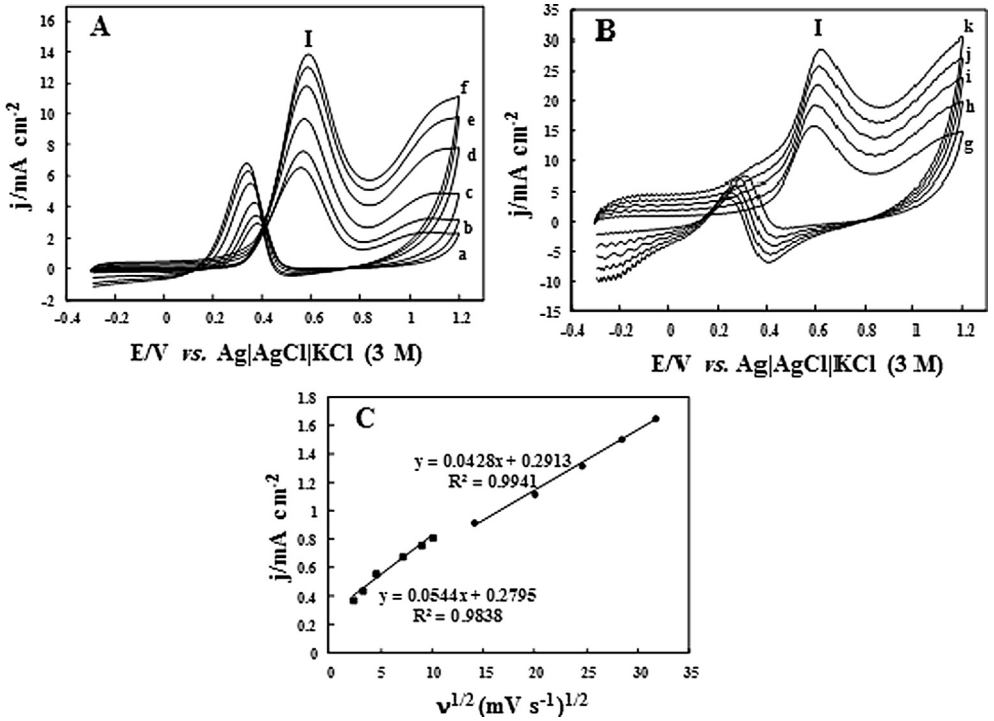

Fig. 11. Cyclic voltammograms of the Pt–Co/G/GCE in 0.5 M H_2SO_4 + 1.0 M methanol aqueous solutions; (A) at lower values of ν: (a) 5, (b) 10, (c) 20, (d) 50, (e) 80, (f) 100 mV s^{-1} and (B) at higher values of ν: (g) 200, (h) 400, (i) 600, (j) 800, (k) 1000 mV s^{-1}. (C) The dependency of the anodic peak current density obtained from (A) and (B) *vs.* $\nu^{1/2}$.

state current density. It is obvious that the Pt–Co/G/GCE exhibits a good stability during methanol electrooxidation.

3.7. Methanol electrooxidation at various switching potentials

In this experiment, the upper potential limit was changed and methanol electrooxidation was recorded. As can be seen in Fig. 10, by increasing the switching potential, the peak current density in forward scan remains relatively unchanged, whereas the peak current density in the reverse scan decreases. As mentioned elsewhere [53], this could be attributed to the formation of Pt oxide. At lower switching potential, Pt oxide formation is prevented, so the electrode surface is relatively clean and higher peak current density is obtained.

3.8. Effect of scan rate on methanol electrooxidation

Electrocatalytic behavior of Pt–Co/G/GCE toward methanol electrooxidation was investigated at different scan rates by cyclic voltammetry (Fig. 11A: 5–100 mV s^{-1}, Fig. 11B: 200–1000 mV s^{-1}). The peak current density versus $\nu^{1/2}$ is linear (Fig. 11C). As can be seen in Fig. 11C, there is a dual linear region. This behavior has been reported in the literature previously [53,57,58]. This behavior can be caused by decreasing rate of methanol diffusion to electrode surface at higher scan rates. Moreover, CO_2 production increases at higher scan rates. Thus, more electrolyte will be expelled from the surface of the electrode. This in turn decreases the number of available sites of catalyst for electrochemical reaction.

4. Conclusion

In summary, Co electrodeposition on graphene modified GC electrode was performed. Then, by replacement reaction, Co was partially replaced by Pt at Co/G/GCE. The fabricated Pt–Co/G/GCE showed electrocatalytic behavior toward methanol electrooxidation. The studies revealed that the existence of graphene nanosheets improved the electrocatalytic behavior of modified electrode. Furthermore, long-term stability of the modified electrodes was studied and it has been found that Pt–Co/G/GCE showed a maximum stability toward methanol oxidation. On the other hand, a linear relationship between the anodic peak current and $\nu^{1/2}$ was observed. This implies that the electrooxidation of methanol at the surface of this modified electrode may be controlled by diffusion process.

References

[1] S. Wang, S.P. Jiang, X. Wang, J. Guo, Electrochim. Acta 56 (2011) 1563–1569.
[2] A.S. Aricò, S. Srinivasan, V. Antonucci, Fuel Cells 1 (2001) 133–161.
[3] S. Wang, X. Wang, S.P. Jiang, Langmuir 24 (2008) 10505–10512.
[4] E. You, R. Guzmán-Blas, E. Nicolau, M. Aulice Scibioh, C.F. Karanikas, J.J. Watkins, C.R. Cabrera, Electrochim. Acta 75 (2012) 191–200.
[5] Y. Sun, Y. Xia, J. Am. Chem. Soc. 126 (2004) 3892–3901.
[6] C. Yee, M. Scotti, A. Ulman, H. White, M. Rafailovich, J. Sokolov, Langmuir 15 (1999) 4314–4316.
[7] M. Hasan, D. Bethell, M. Brust, J. Am. Chem. Soc. 124 (2002) 1132–1133.
[8] D. Rautaray, P.S. Kumar, P.P. Wadgaonkar, M. Sastry, Chem. Mater. 16 (2004) 988–993.
[9] J. Huang, Z. Liu, C. He, L.M. Gan, J. Phys. Chem. B 109 (2005) 16644–16649.
[10] H.A. Gasteiger, N. Markovic, P.N. Ross, E.J. Cairns, J. Phys. Chem. 98 (1994) 617–625.
[11] A.N. Gavrilov, E.R. Savinova, P.A. Simonov, V.I. Zaikovskii, S.V. Cherepanova, G.A. Tsirlina, V.N. Parmon, Phys. Chem. Chem. Phys. 9 (2007) 5476–5489.
[12] W. Chen, J. Kim, S. Sun, S. Chen, J. Phys. Chem. C 112 (2008) 3891–3898.
[13] B.J. Hwang, S.M.S. Kumar, C.-H. Chen, Monalisa, M.-Y. Cheng, D.-G. Liu, J.-F. Lee, J. Phys. Chem. C 111 (2007) 15267–15276.
[14] S. Koh, J. Leisch, M.F. Toney, P. Strasser, J. Phys. Chem. C 111 (2007) 3744–3752.
[15] M.-C. Tsai, T.-K. Yeh, C.-H. Tsai, Int. J. Hydrogen Energy 36 (2011) 8261–8266.
[16] W. He, J. Liu, Y. Qiao, Z. Zou, X. Zhang, D.L. Akins, H. Yang, J. Power Sources 195 (2010) 1046–1050.
[17] C. Xu, L. Wang, X. Mu, Y. Ding, Langmuir 26 (2010) 7437–7443.
[18] K.-T. Jeng, C.-C. Chien, N.-Y. Hsu, S.-C. Yen, S.-D. Chiou, S.-H. Lin, W.-M. Huang, J. Power Sources 160 (2006) 97–104.
[19] L. Li, Y. Xing, J. Phys. Chem. C 111 (2007) 2803–2808.
[20] Q. Huang, H. Yang, Y. Tang, T. Lu, D.L. Akins, Electrochem. Commun. 8 (2006) 1220–1224.
[21] S. Koh, M.F. Toney, P. Strasser, Electrochim. Acta 52 (2007) 2765–2774.
[22] E.B. Fox, H.R. Colon-Mercado, Int. J. Hydrogen Energy 35 (2010) 3280–3286.
[23] J.-S. Yu, S. Kang, S.B. Yoon, G. Chai, J. Am. Chem. Soc. 124 (2002) 9382–9383.
[24] Y. Xin, J.-g. Liu, Y. Zhou, W. Liu, J. Gao, Y. Xie, Y. Yin, Z. Zou, J. Power Sources 196 (2011) 1012–1018.
[25] Y. Zhang, Y.-e. Gu, S. Lin, J. Wei, Z. Wang, C. Wang, Y. Du, W. Ye, Electrochim. Acta 56 (2011) 8746–8751.
[26] B. Luo, S. Xu, X. Yan, Q. Xue, J. Power Sources 205 (2012) 239–243.
[27] K.S. Novoselov, A.K. Geim, S.V. Morozov, D. Jiang, Y. Zhang, S.V. Dubonos, I.V. Grigorieva, A.A. Firsov, Science 306 (2004) 666–669.
[28] A. Rochefort, J.D. Wuest, Langmuir 25 (2009) 210–215.
[29] J. Lu, I. Do, L.T. Drzal, R.M. Worden, I. Lee, ACS Nano 2 (2008) 1825–1832.
[30] Y.G. Zhou, J.J. Chen, F.B. Wang, Z.H. Sheng, X.H. Xia, Chem. Commun. 46 (2010) 5951–5953.
[31] D. Niwa, T. Homma, T. Osaka, J. Phys. Chem. B 108 (2004) 9900–9904.
[32] L. Magagnin, R. Maboudian, C. Carraro, J. Phys. Chem. B 106 (2001) 401–407.
[33] L. Chen, Y. Liu, J. Colloid Interface Sci. 364 (2011) 100–106.
[34] C. Carraro, L. Magagnin, R. Maboudian, Electrochim. Acta 47 (2002) 2583–2588.
[35] G. Kokkinidis, A. Papoutsis, D. Stoychev, A. Milchev, J. Electroanal. Chem. 486 (2000) 48–55.
[36] L.A. Porter, H.C. Choi, A.E. Ribbe, J.M. Buriak, Nano Lett. 2 (2002) 1067–1071.
[37] Z. Wang, T. Ida, H. Sakaue, S. Shingubara, T. Takahagi, Electrochem. Solid-State Lett. 6 (2003) C38–C41.
[38] S.S. Djokić, J. Electrochem. Soc. 143 (1996) 1300–1305.
[39] D.A. Hutt, C. Liu, P.P. Conway, D.C. Whalley, S.H. Mannan, IEEE Trans. Comp. Packag. Technol. 25 (2002) 87–97.
[40] H. Watanabe, H. Honma, J. Electrochem. Soc. 144 (1997) 471–476.
[41] D. Wang, T. Li, Y. Liu, J. Huang, T. You, Cryst. Growth Des. 9 (2009) 4351–4355.
[42] G. Ennas, A. Falqui, S. Marras, C. Sangregorio, G. Marongiu, Chem. Mater. 16 (2004) 5659–5663.
[43] L. Qu, L. Dai, E. Osawa, J. Am. Chem. Soc. 128 (2006) 5523–5532.
[44] A. Ott, S.K. Bhargava, A.P. O'Mullane, Surf. Sci. 606 (2012) L5–L9.
[45] S. Mabbott, I.A. Larmour, V. Vishnyakov, Y. Xu, D. Graham, R. Goodacre, Analyst 137 (2012) 2791–2798.
[46] Y.-C. Liu, S.-J. Yang, Electrochim. Acta 52 (2007) 1925–1931.
[47] W.S. Hummers, R.E. Offernan, J. Am. Chem. Soc. 80 (1958) 1339.
[48] J. Luo, S. Jiang, H. Zhang, J. Jiang, X. Liu, Anal. Chim. Acta 709 (2012) 47–53.
[49] Y. Song, Z. He, H. Zhu, H. Hou, L. Wang, Electrochim. Acta 58 (2011) 757–763.
[50] W. Chartarrayawadee, S.E. Moulton, D. Li, C.O. Too, G.G. Wallace, Electrochim. Acta 60 (2012) 213–223.
[51] Y. Hu, Q. Shao, P. Wu, H. Zhang, C. Cai, Electrochem. Commun. 18 (2012) 96–99.
[52] G.-J. Wang, Y.-Z. Gao, Z.-B. Wang, C.-Y. Du, J.-J. Wang, G.-P. Yin, J. Power Sources 195 (2010) 185–189.
[53] J.-B. Raoof, R. Ojani, S.R. Hosseini, Int. J. Hydrogen Energy 36 (2011) 52–63.
[54] B. Habibi, M.H. Pournaghi-Azar, H. Abdolmohammad-Zadeh, H. Razmi, Int. J. Hydrogen Energy 34 (2009) 2880–2892.
[55] D.-J. Guo, S.-K. Cui, J. Colloid Interface Sci. 340 (2009) 53–57.
[56] J. Qian, W. Wei, X. Huang, Y. Tao, K. Chen, X. Tang, J. Power Sources 210 (2012) 345–349.
[57] W. Zhou, C. Zhai, Y. Du, J. Xu, P. Yang, Int. J. Hydrogen Energy 34 (2009) 9316–9323.
[58] Z. He, J. Chen, D. Liu, H. Zhou, Y. Kuang, Diamond Relat. Mater 13 (2004) 1764–1770.
[59] L. Niu, Q. Li, F. Wei, S. Wu, P. Liu, X. Cao, J. Electroanal. Chem. 578 (2005) 331–337.
[60] M. Hepel, J. Electrochem. Soc. 145 (1998) 124–134.
[61] Z.-F. Chen, Y.-X. Jiang, Y. Wang, J.-M. Xu, L.-Y. Jin, S.-G. Sun, J. Solid State Electrochem. 9 (2005) 363–370.
[62] Y.-B. He, G.-R. Li, Z.-L. Wang, Y.-N. Ou, Y.-X. Tong, J. Phys. Chem. C 114 (2010) 19175–19181.
[63] C. Jiang, X. Lin, J. Power Sources 164 (2007) 49–55.
[64] D.-J. Guo, H.-L. Li, J. Electroanal. Chem. 573 (2004) 197–202.
[65] J. Shen, B. Yan, M. Shi, H. Ma, N. Li, M. Ye, Mater. Res. Bull. 47 (2012) 1486–1493.
[66] G. García, J. Florez-Montaño, A. Hernandez-Creus, E. Pastor, G.A. Planes, J. Power Sources 196 (2011) 2979–2986.